mathematics

Article

Combination of Multigrid with Constraint Data for Inverse Problem of Nonlinear Diffusion Equation

Tao Liu [1,2,*], Di Ouyang [1], Lianjun Guo [3], Ruofeng Qiu [3], Yunfei Qi [3], Wu Xie [3], Qiang Ma [4] and Chao Liu [1]

1 School of Mathematics and Statistics, Northeastern University at Qinhuangdao, Qinhuangdao 066004, China
2 School of Electrical and Electronic Engineering, Nanyang Technological University, Singapore 639798, Singapore
3 Eighth Geological Brigade of Hebei Bureau of Geology and Mineral Resources Exploration, Qinhuangdao 066000, China
4 Department of Mathematics, Harbin Institute of Technology at Weihai, Weihai 264209, China
* Correspondence: liutao@neuq.edu.cn or tao.liu@ntu.edu.sg or math.taoliu@gmail.com

Abstract: This paper delves into a rapid and accurate numerical solution for the inverse problem of the nonlinear diffusion equation in the context of multiphase porous media flow. For the realization of this, the combination of the multigrid method with constraint data is utilized and investigated. Additionally, to address the ill-posedness of the inverse problem, the Tikhonov regularization is incorporated. Numerical results demonstrate the computational performance of this method. The proposed combination strategy displays remarkable capabilities in reducing noise, avoiding local minima, and accelerating convergence. Moreover, this combination method performs better than any one method used alone.

Keywords: inverse problem; nonlinear diffusion equation; multigrid method; constraint data; regularization

MSC: 35R30; 65M55; 76R50; 86A22

Citation: Liu, T.; Ouyang, D.; Guo, L.; Qiu, R.; Qi, Y.; Xie, W.; Ma, Q.; Liu, C. Combination of Multigrid with Constraint Data for Inverse Problem of Nonlinear Diffusion Equation. *Mathematics* **2023**, *11*, 2887. https://doi.org/10.3390/math11132887

Academic Editor: Simeon Reich

Received: 8 May 2023
Revised: 16 June 2023
Accepted: 26 June 2023
Published: 27 June 2023

1. Introduction

In the sense of Hadamard [1], a problem is deemed well-posed when the solution (1) exists, (2) is unique, and (3) is stable (the solution depends continuously on the given data). If one or more of these conditions are not fulfilled then the problem is called ill-posed, while the violations of existence and uniqueness can, to some extent, be decreased by using a minor reformulation of the problem. Violations of stability are much more daunting to handle since they entail that a small disturbance in the data (e.g., noise) may turn out a significant disturbance in the solution to be estimated [2–5].

In general, the inverse problems of diffusion equations are ill-posed, that is, their solution does not fulfill the requirement of the aforementioned conditions in the presence of a tiny disturbance to the input data. To overcome such difficulties, a variety of methods have been proposed [6–12]. To date, considerable efforts have been devoted to formulating accurate and efficient methods of inverse diffusion problems. For example, Rodrigues et al. [13] employed a conjugate gradient method coupled with an adjoint problem formulation to simultaneously determine the source term distribution and diffusion coefficient for a one-dimensional nonlinear diffusion problem. Rashedi [14] tackled an inverse diffusion problem by using operational matrices of orthonormal polynomials. Lukyanenko et al. [15] used an asymptotic-numerical method and location of moving front data to identify the coefficients of the inverse problem for a nonlinear singularly perturbed two-dimensional reaction-diffusion equation. Note that the success of these methods critically hinges on two factors: (1) understanding the specific challenges posed by the inverse problems, and (2) solving the mathematical problems that characterize the properties of these inverse problems.

Based on a nonlinear diffusion equation as the forward problem, one can formulate the inverse problem of determining the unknown parameter from indirect measured data as a nonlinear operator equation. The iteration methods, such as Landweber [16,17], Levenberg–Marquardt [18,19], and Gauss–Newton [20,21], are a natural manner to solve such equations. However, iteration methods were hindered by issues such as initial guess, complexity, and convergence. Theoretical convergence analyses and numerical experiments have demonstrated that these methods have a slow convergence rate and are susceptible to becoming trapped in a local minimum. Additionally, direct implementations suffer from prohibitive memory and computational costs, rendering them unsuitable for large-scale problems. The multigrid method, developed from efforts to overcome these difficulties, has been proven to be effective to enhance convergence rates and avoid local minimum traps when used in conjunction with relaxation or iteration methods for solving nonlinear inverse problems.

The multigrid method is a potent multiscale strategy for conquering a range of calculation difficulties, including slow convergence in iteration and smooth error components. Any large-scale nonlinear problem can be discretized into multiple scales. The multigrid method recursively constructs a series of grids with increasingly coarser scales, combining individual iterations at each grid with diverse inter-grid interactions. Due to interactions between coarse and fine grids, the iteration of the original fine grid problem can rapidly converge to the solution. The multigrid method has been a dynamic approach for solving forward problems of partial differential equations [22–25]. More recently, this method has been utilized to address inverse problems in various fields such as heat transfer [26,27], optical imaging [28–31], biomedical science [32–34], fluids in porous media [35], and economics [36,37].

Nevertheless, achieving preferable application in large complex inverse problems remains a challenge. Under most circumstances, the extremely low signal-to-noise ratio in the measured data can cause enormous errors in the inversion results. To avoid amplifying noises attributable to the ill-posedness of the inverse problems, the constraint condition is introduced. Including constraint data results in a unique and stable solution for the inverse problem pertaining to the data, thereby transforming the initially ill-posed problem into a well-posed one [38]. In addition, the constraint data have lower noise since they were obtained from the interior of the actual model, which can reduce the disturbance of noise and improve inversion quality. Many applications related to the constraint condition have been developed in the area of inverse problems [39–42].

The present study puts forth a fresh methodology that employs multigrid iteration and constraint data to surmount the inverse problem of the nonlinear diffusion equation. This methodology can enhance the convergence rate and improve the robustness to noise. We consider the following permeability identification model of the nonlinear diffusion equation in the multiphase porous media flow:

$$u_t - \nabla \cdot (\theta(\mathbf{x})\Phi(u, \nabla u)\nabla u) = \eta(\mathbf{x}, t), \quad (\mathbf{x}, t) \in \Omega \times (0, T), \tag{1}$$

with the boundary and the initial conditions

$$u(\mathbf{x}, t) = 0, \quad (\mathbf{x}, t) \in \partial\Omega \times (0, T), \tag{2}$$

$$u(\mathbf{x}, 0) = \xi(\mathbf{x}), \quad \mathrm{x} \in \Omega, \tag{3}$$

subject to the additional condition

$$u(\mathbf{x}_h, t) = \lambda(\mathbf{x}_h, t), \quad h = 1, 2, \ldots, H, \quad t \in (0, T), \tag{4}$$

where θ is the unknown permeability, Φ is the positive nonlinear diffusion function of u or ∇u, η is the source function, and λ is the measured data. For brevity, the domain Ω is assumed to be a unit square. Equations (1)–(4) can be simplified into a nonlinear operator equation using the finite-difference method. The permeability and measured data can then be placed into the vectors $\mathbf{\Theta}$ and $\mathbf{\Lambda}$, yielding:

$$\Psi(\mathbf{\Theta}) = \mathbf{\Lambda}. \tag{5}$$

Moreover, we impose the constraints, and hence Equation (5) can be reformulated as a nonlinear constrained optimization problem

$$\min_{\mathbf{\Theta}} \|\Psi(\mathbf{\Theta}) - \overline{\mathbf{\Lambda}}\|^2, \quad \text{subject to } A\mathbf{\Theta} = \overrightarrow{\mathbf{\Theta}}_{i'}, \tag{6}$$

where A is a large information matrix indicating where the constraints exist, $\overrightarrow{\mathbf{\Theta}}_{i'}$ is the constraint data such as well logs, and the vector $\overline{\mathbf{\Lambda}}$ represents known error-included measured data, which can be denoted as the following:

$$\overline{\mathbf{\Lambda}} = \mathbf{\Lambda} + \varepsilon,$$

where ε represents the error in $\overline{\mathbf{\Lambda}}$ that may come from measurement and/or discretization process.

In the following theorem, the existence conditions of exact solution for direct problem (1)–(3) are provided. For more details about the solution existence of both the direct and inverse problems, the interested readers may refer to [43–49].

Theorem 1. *Assume that $\theta(\mathbf{x})\Phi(u, \nabla u)\nabla u$ is a Carathéodory function satisfying the classical Leray–Lions structure conditions [43]. Let $\frac{2\mathbf{N}+1}{\mathbf{N}+1} < \mathbf{p} < \mathbf{N}$ and ρ be such that*

$$1 < \rho < \bar{\rho} = (\mathbf{p}^*)' = \frac{\mathbf{N}\mathbf{p}}{\mathbf{N}\mathbf{p} - \mathbf{N} + \mathbf{p}},$$

where $\mathbf{N}$ is the dimension of Ω, and $\mathbf{p}^*$ is the Sobolev conjugate exponent of $\mathbf{p}$ ($\mathbf{p}^* = \frac{\mathbf{N}\mathbf{p}}{\mathbf{N}-\mathbf{p}}$). Then, there exists a constant $\bar{\sigma} = \bar{\sigma}(\rho)$ satisfying

$$\rho < \bar{\sigma} < \frac{\mathbf{p}(\rho + \mathbf{N}) - \rho\mathbf{N}}{\mathbf{p}(\rho + \mathbf{N}) - 2\mathbf{N}},$$

such that the following holds: if

$$1 \le \sigma < \bar{\sigma}, \quad \kappa = \rho + (\sigma - 1)\left(\frac{\rho + \mathbf{N}}{\mathbf{N}}\mathbf{p} - 2\right)$$

and

$$\eta \in L^{\sigma}(0, T; L^{\rho}(\Omega)), \quad \xi \in L^{\kappa}(\Omega),$$

then there exists a solution u of direct problem (1)–(3) such that

$$u \in L^{\mathbf{q}}(0, T; W_0^{1,\mathbf{q}}(\Omega)),$$

where $\mathbf{q} = \sigma\mathbf{p} + \frac{(\rho - 2\sigma)\mathbf{N}}{\rho + \mathbf{N}}$.

Equation (6) can be transformed into an unconstrained optimization problem by constructing penalty terms, where the constraints are converted into the form of penalty functions. The proposed method in this study is the use of the multigrid method, with an iterative method as the relaxation factor for grid correction and smoothing, to obtain an accurate and fast solution for Equation (5).

The remainder of the paper is structured as follows: In the next section, we adopt the finite-difference method to solve the forward problem; describe the inverse problem with constraints under a discrete setting; and give the iterative method. Section 3 describes and illustrates in detail the V-cycle multigrid method. Numerical results demonstrating the performance of the method are presented in Section 4, followed by the conclusions in Section 5.

2. Inversion Framework and Iterative Method

Given the forward problem defined in Equations (1)–(3), we define Δt as the discretization interval in the temporal dimension, while Δx and Δy represent the discretization intervals of the rectangular grid along the horizontal and vertical directions in the spatial dimension, respectively. The problem can be discretized with the finite-difference method:

$$\begin{cases} \frac{u_{i,j}^n - u_{i,j}^{n-1}}{\Delta t} - \nabla \cdot \left(\theta_{i,j} \Phi_{i,j}^n \nabla u_{i,j}^n \right) = \eta_{i,j}^n, \\ i = 1, 2, \ldots, K_1 - 1; \quad j = 1, 2, \ldots, K_2 - 1; \quad n = 1, 2, \ldots, K_3, \\ u_{i,0}^n = u_{i,K_2}^n = 0, \quad i = 0, 1, \ldots, K_1, \\ u_{0,j}^n = u_{K_1,j}^n = 0, \quad j = 0, 1, \ldots, K_2, \\ u_{i,j}^0 = \xi_{i,j}, \quad i = 0, 1, \ldots, K_1; \quad j = 0, 1, \ldots, K_2, \\ u_{\mathbf{x}_h}^n = \lambda_{\mathbf{x}_h}^n, \quad h = 1, 2, \ldots, H; \quad n = 1, 2, \ldots, K_3, \end{cases} \tag{7}$$

where

$$\begin{aligned} &u_{i,j}^n = u(i\Delta x, j\Delta y, n\Delta t), \quad \eta_{i,j}^n = \eta(i\Delta x, j\Delta y, n\Delta t), \\ &\theta_{i,j} = \theta(i\Delta x, j\Delta y), \quad \xi_{i,j} = \xi(i\Delta x, j\Delta y), \quad \lambda_{\mathbf{x}_h}^n = \lambda(\mathbf{x}_h, n\Delta t), \\ &K_1 = 1/\Delta x, \quad K_2 = 1/\Delta y, \quad K_3 = T/\Delta t, \end{aligned}$$

$\nabla \cdot \left(\theta_{i,j} \Phi_{i,j}^n \nabla u_{i,j}^n \right)$ is the discrete form of the nonlinear diffusion term, which can be found in reference [50]. Subsequently, Equation (7) can construct the nonlinear operator Equation (5), and

$$\begin{aligned} \mathbf{\Theta}^\top &= \left(\theta_{1,1}, \theta_{1,2}, \ldots, \theta_{1,K_2}, \theta_{2,1}, \theta_{2,2}, \ldots, \theta_{2,K_2}, \ldots, \theta_{K_1,1}, \theta_{K_1,2}, \ldots, \theta_{K_1,K_2} \right), \\ \mathbf{\Lambda}^\top &= \left(\lambda_{\mathbf{x}_1}^1, \lambda_{\mathbf{x}_2}^1, \ldots, \lambda_{\mathbf{x}_H}^1, \lambda_{\mathbf{x}_1}^2, \lambda_{\mathbf{x}_2}^2, \ldots, \lambda_{\mathbf{x}_H}^2, \ldots, \lambda_{\mathbf{x}_1}^{K_3}, \lambda_{\mathbf{x}_2}^{K_3}, \ldots, \lambda_{\mathbf{x}_H}^{K_3} \right). \end{aligned}$$

The objective of the considered inverse problem is to infer the unknown parameter $\theta(\mathbf{x})$ using the noisy measured data $\overline{\lambda}_{\mathbf{x}_h}^n$, which can be placed into the vector $\overline{\mathbf{\Lambda}}$ with the same sequence as $\mathbf{\Lambda}$. Consequently, the inverse problem can be reformulated into an optimization problem represented by

$$\min_{\mathbf{\Theta}} \| \Psi(\mathbf{\Theta}) - \overline{\mathbf{\Lambda}} \|^2. \tag{8}$$

To enhance the quality of parameter identification for the inverse problem with an extremely low signal-to-noise ratio, it may prove advantageous to employ constraint data, such as internal data with a high signal-to-noise ratio. As such, in the aforementioned Equation (8), the parameter $\mathbf{\Theta}$ can be constrained with some known permeability $\overrightarrow{\mathbf{\Theta}}_{i'}$ derived from the well logs of a well situated at point i' in the horizontal direction. Specifically, we have

$$\overrightarrow{\mathbf{\Theta}}_{i'}^\top = \left(\overrightarrow{\theta}_{i',1}, \overrightarrow{\theta}_{i',2}, \ldots, \overrightarrow{\theta}_{i',K_2} \right).$$

Let A be the matrix

$$A = \begin{bmatrix} 0 & 0 & \cdots & 0 & 1 & 0 & \cdots & 0 & 0 & 0 & \cdots & 0 \\ 0 & 0 & \cdots & 0 & 0 & 1 & \cdots & 0 & 0 & 0 & \cdots & 0 \\ \vdots & \vdots & & \vdots & \vdots & \vdots & \ddots & \vdots & \vdots & \vdots & & \vdots \\ 0 & 0 & \cdots & 0 & 0 & 0 & \cdots & 1 & 0 & 0 & \cdots & 0 \end{bmatrix}_{K_2 \times (K_1 \times K_2)}$$

such that $A\boldsymbol{\Theta} = \left(\theta_{i',1}, \theta_{i',2}, \ldots, \theta_{i',K_2}\right)^\top$, and $\boldsymbol{\Theta}$ satisfy the constraint set containing the known permeability

$$\Xi = \left\{\boldsymbol{\Theta} : \theta_{i',j} = \overrightarrow{\theta}_{i',j}, j = 1, 2, \ldots, K_2\right\},$$

Equation (8) then turns into the following constrained optimization problem:

$$\min_{\boldsymbol{\Theta}\in\Xi} \|\Psi(\boldsymbol{\Theta}) - \overline{\boldsymbol{\Lambda}}\|^2, \tag{9}$$

where $\boldsymbol{\Theta} \in \Xi$ implies that $A\boldsymbol{\Theta} - \overrightarrow{\boldsymbol{\Theta}}_{i'} = 0$. So, the constraint condition can be replaced by a penalty term, and Equation (9) can be further rewritten as an optimization problem without constraints

$$\min_{\boldsymbol{\Theta}}\left\{\|\Psi(\boldsymbol{\Theta}) - \overline{\boldsymbol{\Lambda}}\|^2 + \nu\|A\boldsymbol{\Theta} - \overrightarrow{\boldsymbol{\Theta}}_{i'}\|^2\right\}, \tag{10}$$

where ν is the penalty parameter. To ensure that the solution of Equation (10) closely approximates the one of Equation (9), a sufficiently large penalty parameter ν needs to be selected.

To address the intrinsic ill-posed nature of the inverse problem, some regularization methods must be included. We introduce Tikhonov regularization, which involves the addition of second-order smoothing matrices B_1 and B_2 in the horizontal and vertical directions, each with corresponding regularized parameters μ_1 and μ_2. With these regularization terms in place, the inverse problem is converted to

$$\min_{\boldsymbol{\Theta}}\left\{\|\Psi(\boldsymbol{\Theta}) - \overline{\boldsymbol{\Lambda}}\|^2 + \nu\|A\boldsymbol{\Theta} - \overrightarrow{\boldsymbol{\Theta}}_{i'}\|^2 + \mu_1\|B_1\boldsymbol{\Theta}\|^2 + \mu_2\|B_2\boldsymbol{\Theta}\|^2\right\}. \tag{11}$$

By the derivation process of the regularized Gauss–Newton method, an iterative method, which can be utilized to obtain the solution of Equation (11), is given as follows:

$$\begin{aligned}\boldsymbol{\Theta}^{k+1} = \boldsymbol{\Theta}^k - &\left[\Psi'(\boldsymbol{\Theta}^k)^\top\Psi'(\boldsymbol{\Theta}^k) + \nu A^\top A + \mu_1 B_1^\top B_1 + \mu_2 B_2^\top B_2\right]^{-1} \times \\ &\Big[\Psi'(\boldsymbol{\Theta}^k)^\top(\Psi(\boldsymbol{\Theta}^k) - \overline{\boldsymbol{\Lambda}}) + \nu A^\top(A\boldsymbol{\Theta}^k - \overrightarrow{\boldsymbol{\Theta}}_{i'}) + \\ &(\mu_1 B_1^\top B_1 + \mu_2 B_2^\top B_2)\boldsymbol{\Theta}^k\Big], \quad k = 0, 1, 2, \ldots\end{aligned} \tag{12}$$

3. Multigrid Method with Constraints

This section describes in detail how the multigrid method is combined with constraint data to solve the inverse problem of the nonlinear diffusion equation. Let Σ^0 denote the finest grid, and let Σ^q be a coarse resolution representation of Σ^0 with a discretization interval that is 2^q times larger than the finest grid. In order to transfer information between coarse and fine grids, we define the restriction operators

$$\mathbb{H}_q^{q+1} : \Sigma^q \to \Sigma^{q+1}, \quad q = 0, 1, \ldots, Q-1,$$

and corresponding prolongation operators

$$\mathbb{H}_{q+1}^{q} : \Sigma^{q+1} \to \Sigma^q, \quad q = 0, 1, \ldots, Q-1.$$

By discretizing the inverse problem on the grid Σ^q, we have the corresponding objective functional with a form similar to that of Equation (11)

$$\begin{aligned}F^{(q)}(\boldsymbol{\Theta}^{(q)}) = \|\Psi^{(q)}(\boldsymbol{\Theta}^{(q)}) - \overline{\boldsymbol{\Lambda}}^{(q)}\|^2 + \nu^{(q)}\|A^{(q)}\boldsymbol{\Theta}^{(q)} - \overrightarrow{\boldsymbol{\Theta}}_{i'}^{(q)}\|^2 + \\ \mu_1^{(q)}\|B_1^{(q)}\boldsymbol{\Theta}^{(q)}\|^2 + \mu_2^{(q)}\|B_2^{(q)}\boldsymbol{\Theta}^{(q)}\|^2.\end{aligned} \tag{13}$$

Note that coarsening the grid accelerates the convergence speed, but it does not come at the expense of reduced discretization accuracy. To illustrate this, take the example of the two-grid method (see Figure 1).

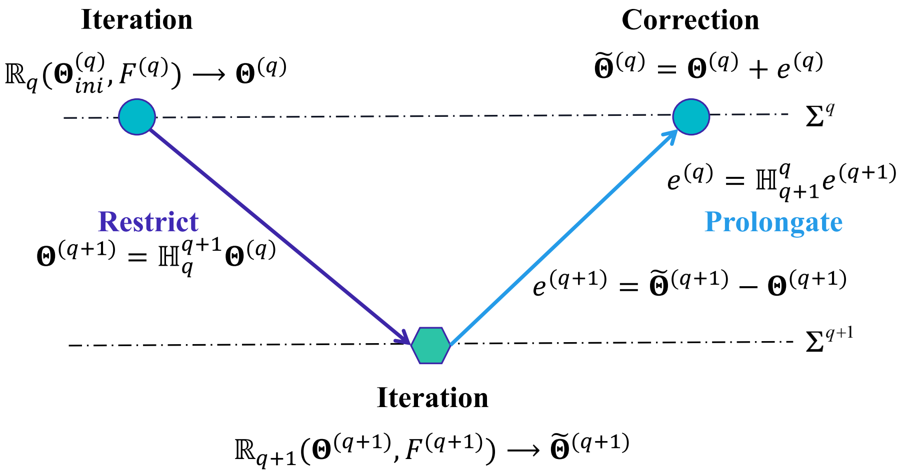

Figure 1. Schematic illustration of the two-grid method.

The initial approximation $\mathbf{\Theta}^{(q)}_{ini}$ is first iterated by the relaxation operator to obtain a new approximation $\mathbf{\Theta}^{(q)}$

$$\mathbf{\Theta}^{(q)} \longleftarrow \mathbb{R}_q(\mathbf{\Theta}^{(q)}_{ini}, F^{(q)}), \tag{14}$$

where $\mathbb{R}_q$ corresponds to the iterative Equation (12), $\mathbf{\Theta}^{(q)}_{ini}$ is the initial guess, and $F^{(q)}$ is the objective functional. Then, the new approximation $\mathbf{\Theta}^{(q)}$ is transferred from the fine grid Σ^q to the coarse grid Σ^{q+1} using the restriction operator, obtaining a coarse grid approximation

$$\mathbf{\Theta}^{(q+1)} = \mathbb{H}^{q+1}_q \mathbf{\Theta}^{(q)}. \tag{15}$$

Next, the relaxation operator performs iterations on the coarse gird Σ^{q+1} to obtain the corrected coarse grid approximation

$$\widetilde{\mathbf{\Theta}}^{(q+1)} \longleftarrow \mathbb{R}_{q+1}(\mathbf{\Theta}^{(q+1)}, F^{(q+1)}). \tag{16}$$

Finally, use the approximation error $e^{(q+1)}$ on the coarse gird to correct the approximation on the fine grid, resulting in

$$\widetilde{\mathbf{\Theta}}^{(q)} = \mathbf{\Theta}^{(q)} + \mathbb{H}^q_{q+1}(\widetilde{\mathbf{\Theta}}^{(q+1)} - \mathbb{H}^{q+1}_q \mathbf{\Theta}^{(q)}). \tag{17}$$

Ideally, the updated approximation $\widetilde{\mathbf{\Theta}}^{(q)}$ is expected to be better than the previous approximation $\mathbf{\Theta}^{(q)}$, that is, $F^{(q)}(\widetilde{\mathbf{\Theta}}^{(q)}) \leq F^{(q)}(\mathbf{\Theta}^{(q)})$. However, this may not be true in the case of inconsistent objective functionals. Figure 2 highlights that the coarse grid correction, in some cases, could cause the approximation to deviate from the optimal solution.

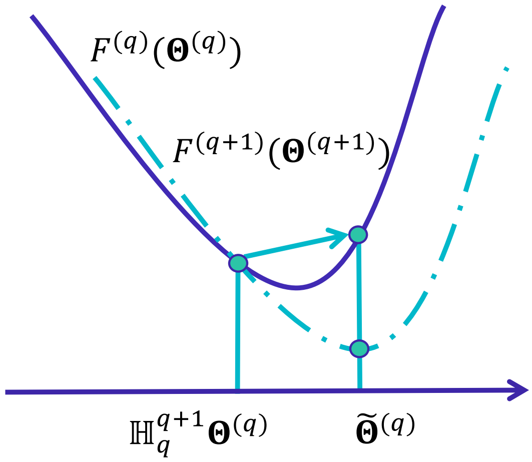

Figure 2. Coarse grid correction causes the approximation to deviate from the optimal solution in general cases.

To this end, we begin by adding a correction term $\beta^{(q)}\boldsymbol{\Theta}^{(q)}$ to the objective functional

$$\begin{aligned} F_\beta^{(q)}(\boldsymbol{\Theta}^{(q)}) &= F^{(q)}(\boldsymbol{\Theta}^{(q)}) - \beta^{(q)}\boldsymbol{\Theta}^{(q)} \\ &= \|\boldsymbol{\Psi}^{(q)}(\boldsymbol{\Theta}^{(q)}) - \overline{\boldsymbol{\Lambda}}^{(q)}\|^2 + \nu^{(q)}\|A^{(q)}\boldsymbol{\Theta}^{(q)} - \overrightarrow{\boldsymbol{\Theta}}_{i'}^{(q)}\|^2 + \\ &\quad \mu_1^{(q)}\|B_1^{(q)}\boldsymbol{\Theta}^{(q)}\|^2 + \mu_2^{(q)}\|B_2^{(q)}\boldsymbol{\Theta}^{(q)}\|^2 - \beta^{(q)}\boldsymbol{\Theta}^{(q)}, \end{aligned} \tag{18}$$

where $\beta^{(q)}$ is aimed at adjusting the functional's gradient, and in the finest grid case, define that $\beta^{(0)} = \mathbf{0}$. Then, the following additional conditions are imposed to ensure the objective functionals matching, which leads to the monotonous convergence of the multigrid method.

C1. The initial errors between the model data and measured data are equal on the coarse and fine grids

$$\boldsymbol{\Psi}^{(q+1)}(\mathbb{H}_q^{q+1}\boldsymbol{\Theta}^{(q)}) - \overline{\boldsymbol{\Lambda}}^{(q+1)} = \boldsymbol{\Psi}^{(q)}(\boldsymbol{\Theta}^{(q)}) - \overline{\boldsymbol{\Lambda}}^{(q)}, \tag{19}$$

then $\overline{\boldsymbol{\Lambda}}^{(q+1)}$ is given by

$$\overline{\boldsymbol{\Lambda}}^{(q+1)} = \overline{\boldsymbol{\Lambda}}^{(q)} - \left[\boldsymbol{\Psi}^{(q)}(\boldsymbol{\Theta}^{(q)}) - \boldsymbol{\Psi}^{(q+1)}(\mathbb{H}_q^{q+1}\boldsymbol{\Theta}^{(q)})\right]. \tag{20}$$

C2. The equal conditions are also valid on the constraint and regularization terms

$$\begin{aligned} &\nu^{(q+1)}\|A^{(q+1)}\mathbb{H}_q^{q+1}\boldsymbol{\Theta}^{(q)} - \overrightarrow{\boldsymbol{\Theta}}_{i'}^{(q+1)}\|^2 = \nu^{(q)}\|A^{(q)}\boldsymbol{\Theta}^{(q)} - \overrightarrow{\boldsymbol{\Theta}}_{i'}^{(q)}\|^2, \\ &\mu_1^{(q+1)}\|B_1^{(q+1)}\mathbb{H}_q^{q+1}\boldsymbol{\Theta}^{(q)}\|^2 = \mu_1^{(q)}\|B_1^{(q)}\boldsymbol{\Theta}^{(q)}\|^2, \\ &\mu_2^{(q+1)}\|B_2^{(q+1)}\mathbb{H}_q^{q+1}\boldsymbol{\Theta}^{(q)}\|^2 = \mu_2^{(q)}\|B_2^{(q)}\boldsymbol{\Theta}^{(q)}\|^2, \end{aligned} \tag{21}$$

$\nu^{(q+1)}, \mu_1^{(q+1)}, \mu_2^{(q+1)}$ can then be written as

$$\begin{aligned} \nu^{(q+1)} &= \frac{\|A^{(q)}\boldsymbol{\Theta}^{(q)} - \overrightarrow{\boldsymbol{\Theta}}_{i'}^{(q)}\|^2}{\|A^{(q+1)}\mathbb{H}_q^{q+1}\boldsymbol{\Theta}^{(q)} - \overrightarrow{\boldsymbol{\Theta}}_{i'}^{(q+1)}\|^2}\nu^{(q)}, \\ \mu_1^{(q+1)} &= \frac{\|B_1^{(q)}\boldsymbol{\Theta}^{(q)}\|^2}{\|B_1^{(q+1)}\mathbb{H}_q^{q+1}\boldsymbol{\Theta}^{(q)}\|^2}\mu_1^{(q)}, \\ \mu_2^{(q+1)} &= \frac{\|B_2^{(q)}\boldsymbol{\Theta}^{(q)}\|^2}{\|B_2^{(q+1)}\mathbb{H}_q^{q+1}\boldsymbol{\Theta}^{(q)}\|^2}\mu_2^{(q)}. \end{aligned} \tag{22}$$

C3. The gradients of the coarse and fine objective functionals ought to be equal, that is,

$$\nabla F_{\beta}^{(q+1)}(\mathbb{H}_q^{q+1}\boldsymbol{\Theta}^{(q)}) = \nabla F_{\beta}^{(q)}(\boldsymbol{\Theta}^{(q)})\mathbb{H}_{q+1}^{q}, \tag{23}$$

which makes sure that the optimal solution is a fixed point of the multigrid method (see Figure 3). Then, applying Equation (23), we have

$$\beta^{(q+1)} = \nabla F^{(q+1)}(\mathbb{H}_q^{q+1}\boldsymbol{\Theta}^{(q)}) - \nabla F_{\beta}^{(q)}(\boldsymbol{\Theta}^{(q)})\mathbb{H}_{q+1}^{q}. \tag{24}$$

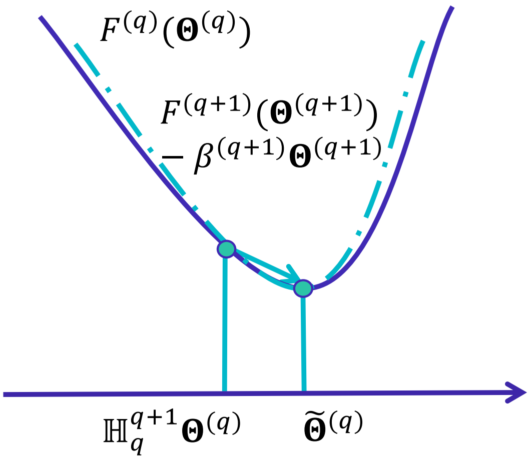

Figure 3. Coarse grid correction causes the approximation to converge to the optimal solution after condition C3 is satisfied.

Ultimately, a stable and convergent V-cycle multigrid method can be constructed by recursively embedding the two-grid method into itself and enforcing conditions C1, C2, and C3 (see Figure 4).

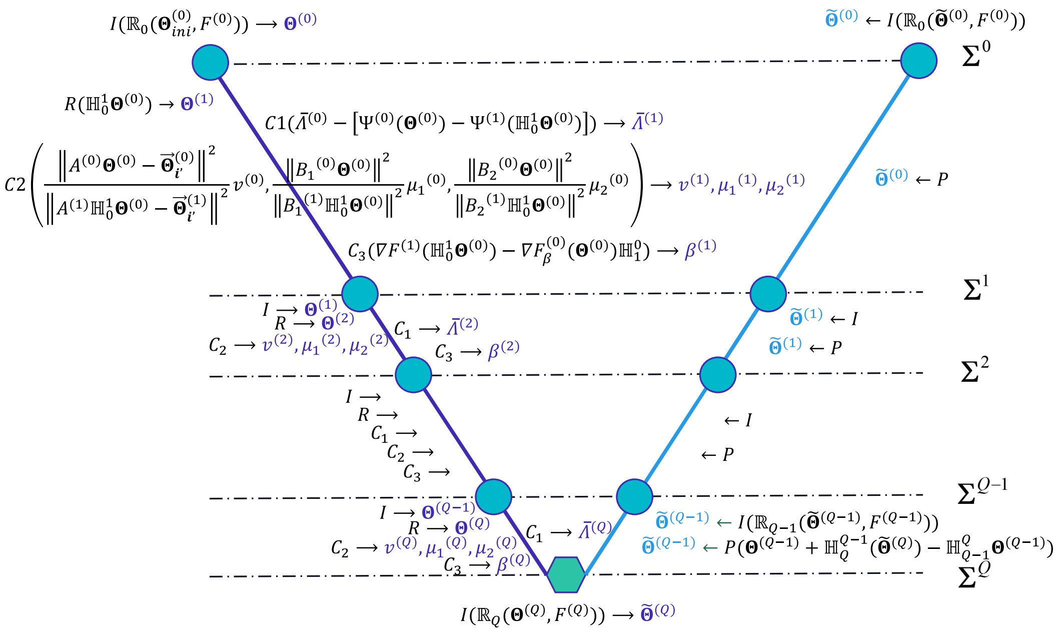

Figure 4. Schematic illustration of the V-cycle multigrid method.

4. Numerical Results

In this section, the results obtained by the proposed method are studied. The inverse problem, modeled by Equations (1)–(4), is solved by assuming $\eta(\mathbf{x}, t) = 0$, $\xi(\mathbf{x}) = \sin(\pi x)\sin(\pi y)$, and $T = 0.06$. The discretization parameters are chosen as $\Delta x = \Delta y = \frac{1}{28}$

and $\Delta t = 0.002$. We choose for the method parameters $i' = \frac{14}{28}$, $\nu = 10^4$, $\mu_1 = \mu_2 = 10^{-6}$, and $\mathbf{\Theta}_{ini}^{(q)} \equiv 5$.

4.1. Example 1

As the first example, consider the nonlinear diffusion function $\Phi(u) = 1 + \frac{1}{2}u + u^2$, and the true model in Figure 5. The numerical experiments are performed by using the multigrid method with constraints (MGMC), multigrid method without constraints (MGM), and fixed-grid method with constraints (FGMC) with 5%, 10%, 15%, and 20% Gaussian noise measured data, respectively. The inversion results generated by the application of MGMC are visually presented in Figures 6–9. Obviously, the proposed method is stable under different levels of noise.

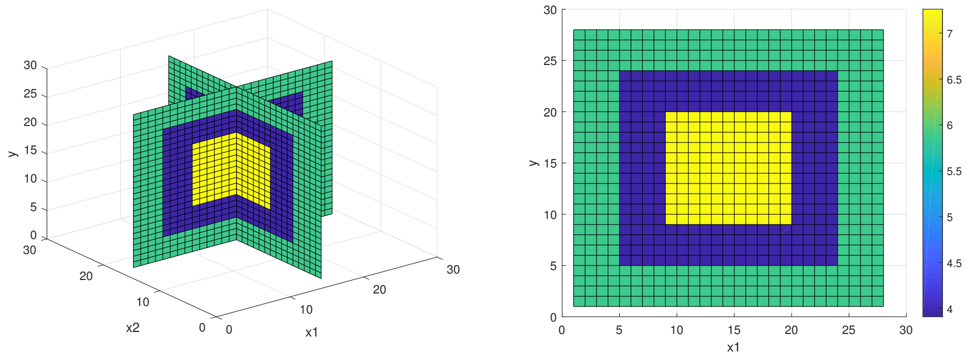

(**a**) 3D model. (**b**) 2D profile.

Figure 5. The 2D and 3D views of the true permeability model in Example 1. The color depicts values of permeability.

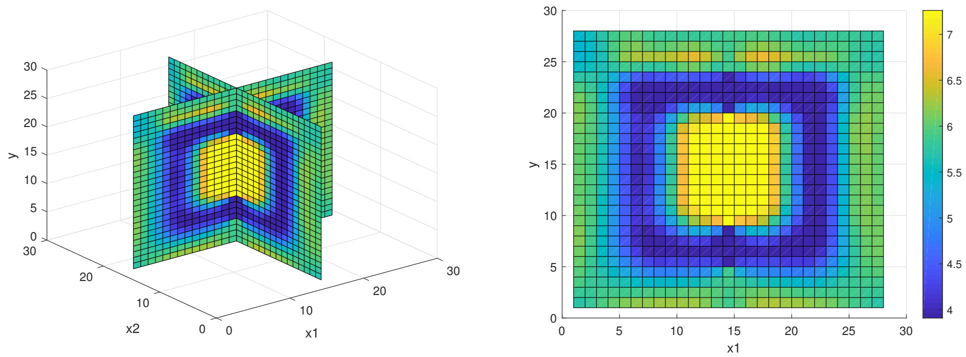

(**a**) 3D model. (**b**) 2D profile.

Figure 6. The 2D and 3D views of MGMC inversion result under 5% noise level in Example 1.

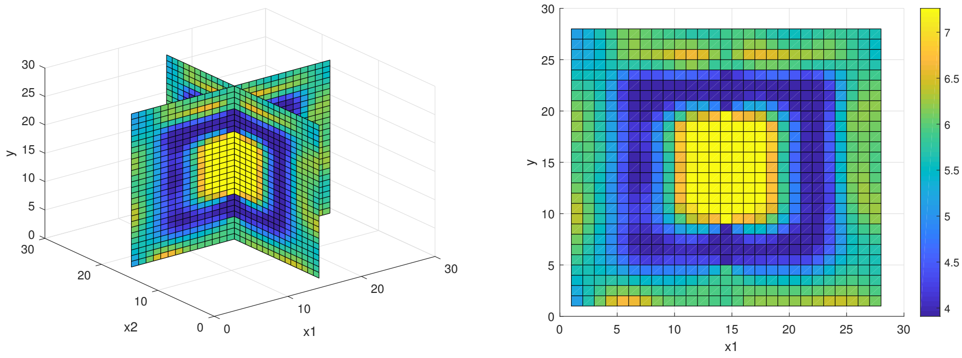

(**a**) 3D model. (**b**) 2D profile.

Figure 7. The 2D and 3D views of MGMC inversion result under 10% noise level in Example 1.

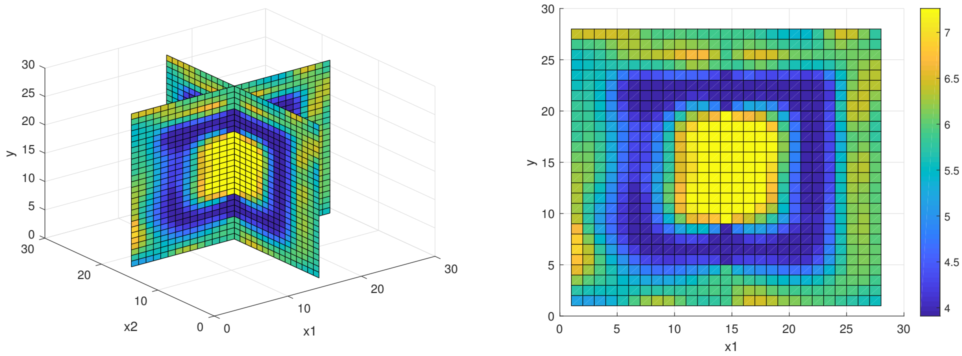

(**a**) 3D model. (**b**) 2D profile.

Figure 8. The 2D and 3D views of MGMC inversion result under 15% noise level in Example 1.

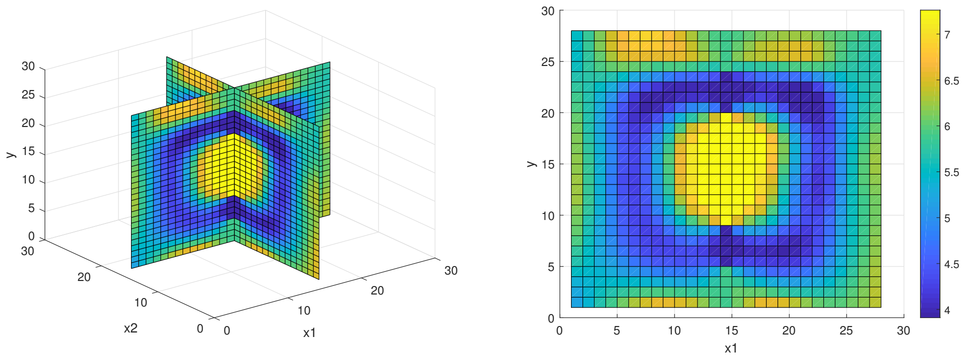

(**a**) 3D model. (**b**) 2D profile.

Figure 9. The 2D and 3D views of MGMC inversion result under 20% noise level in Example 1.

The numerical results of Example 1 are listed in Table 1, which serves as further evidence of the stability of the proposed method. Even as the noise is increased, there is no considerable difference in terms of relative error. When the noise is increased to 15%, MGM leads to divergent solutions, and when the noise reaches 20%, both MGM and FGMC result in divergent solutions. Additionally, Table 1 presents that the computation time of MGMC is substantially lower than that of the other two methods. It is apparent that MGCS has good abilities to suppress noise, avoid local minima, and speed up convergence.

Table 1. Numerical results of Example 1.

	Noise Level	MGMC	MGM	FGMC
Computation times (seconds)	5%	259.7277	290.8756	499.3136
	10%	260.1248	292.8695	504.0138
	15%	264.4826	×	510.7545
	20%	268.3424	×	×
Relative errors	5%	6.64%	8.17%	6.81%
	10%	6.75%	9.11%	7.54%
	15%	7.18%	×	8.67%
	20%	8.31%	×	×

4.2. Example 2

The nonlinear diffusion function $\Phi(\nabla u) = 1 + 0.1|\nabla u|^2$ is considered in this example. To investigate the sensitivity of method to anomalous bodies, we use the true model in Figure 10, which has two anomalous bodies. As demonstrated in Figures 11–14, the inversion results of MGMC are quite satisfactory.

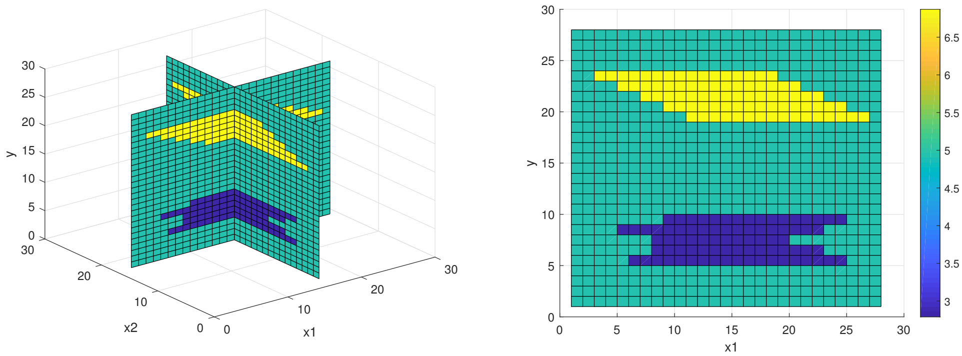

(**a**) 3D model. (**b**) 2D profile.

Figure 10. The 2D and 3D views of the true permeability model in Example 2. The color depicts values of permeability.

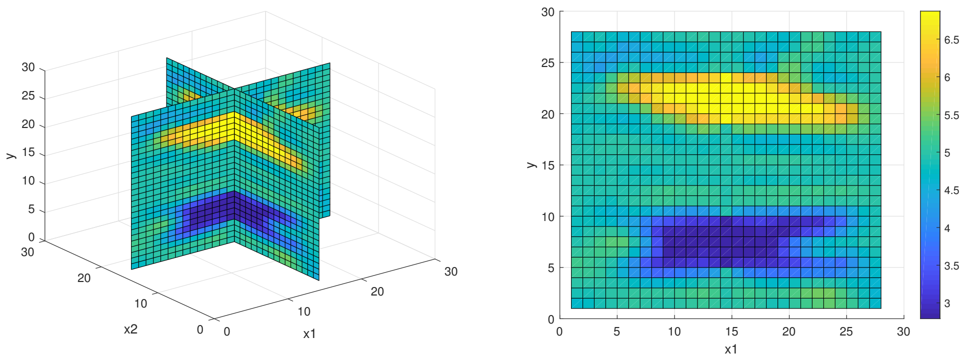

(**a**) 3D model. (**b**) 2D profile.

Figure 11. The 2D and 3D views of MGMC inversion result under 5% noise level in Example 2.

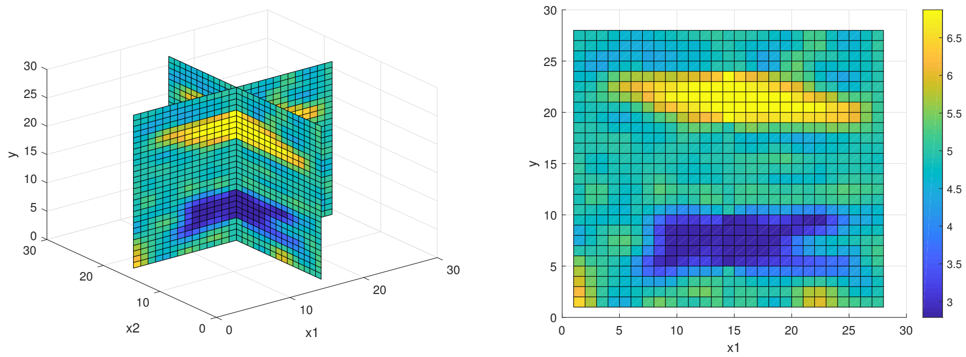

(**a**) 3D model. (**b**) 2D profile.

Figure 12. The 2D and 3D views of MGMC inversion result under 10% noise level in Example 2.

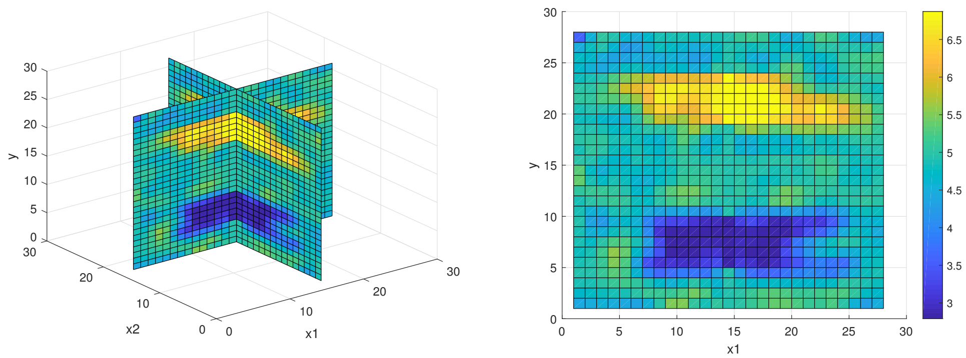

(**a**) 3D model. (**b**) 2D profile.

Figure 13. The 2D and 3D views of MGMC inversion result under 15% noise level in Example 2.

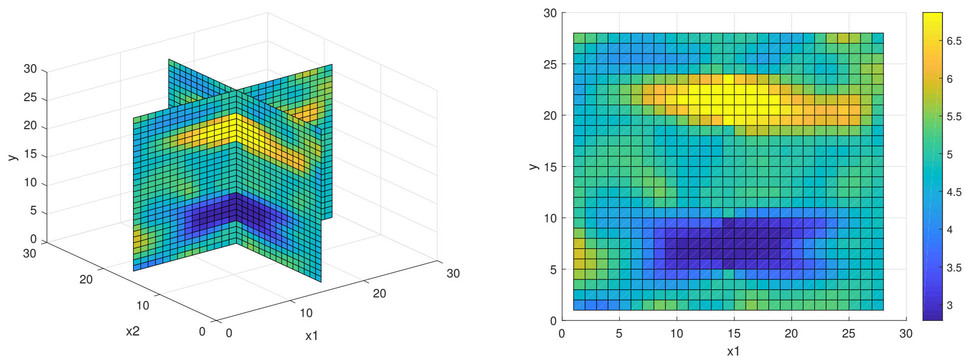

(**a**) 3D model. (**b**) 2D profile.

Figure 14. The 2D and 3D views of MGMC inversion result under 20% noise level in Example 2.

Once again, we conduct a comparison among the aforementioned three methods in terms of computational efficiency and accuracy. The numerical results of Example 2 are listed in Table 2, which shows that MGMC performs best in all cases, has fast computational speed, and has good noise robustness. Given that the method proposed in this study effectively combines the features of multigrid techniques in reducing the influence of local minima with the advantages associated with high signal-to-noise ratio constraint data, it comes as no surprise that this method reduces the disturbance of noise, improves the inversion quality, and remains viable in addressing the challenges posed by anomalous bodies.

Table 2. Numerical results of Example 2.

	Noise Level	MGMC	MGM	FGMC
Computation times (seconds)	5%	331.7824	360.3283	644.5451
	10%	334.5813	366.3703	651.8835
	15%	350.5091	×	×
	20%	393.5369	×	×
Relative errors	5%	4.97%	7.39%	5.16%
	10%	5.13%	8.59%	7.15%
	15%	5.39%	×	×
	20%	6.10%	×	×

5. Conclusions

A combination method using the multigrid technique and constraint data has been employed to solve the inverse problem of the nonlinear diffusion equation in the realm of multiphase porous media flow. Our method provides several notable advantages. Firstly, it uses the high signal-to-noise ratio constraint data and Tikhonov regularization for the associated optimization problem, which greatly overcomes the noise interference and ill-posed property. Secondly, in the presence of multigrid, our method provides fast convergence and good accuracy to find the numerical solution. To evaluate the performance of the proposed method, we consider two illustrative test examples. The numerical results indicate that combining the multigrid with constraint data serves as a stable and efficient tool for accurately identifying the permeability model in multiphase porous media flow.

Author Contributions: Conceptualization, T.L.; methodology, T.L. and D.O.; software, T.L. and D.O.; validation, T.L. and D.O.; formal analysis, T.L. and D.O.; investigation, T.L. and D.O.; resources, L.G., R.Q., Y.Q., and W.X.; data curation, C.L.; writing—original draft preparation, T.L. and D.O.; writing—review and editing, T.L. and D.O.; visualization, Q.M.; supervision, C.L.; project administration, L.G., R.Q., Y.Q. and W.X.; and funding acquisition, L.G., R.Q., Y.Q., and W.X. All authors have read and agreed to the published version of the manuscript.

Funding: This research was funded by the Natural Science Foundation of Hebei Province of China (A2020501007), the Fundamental Research Funds for the Central Universities (N2123015), the Open Fund Project of Marine Ecological Restoration and Smart Ocean Engineering Research Center of Hebei Province (HBMESO2321), and the Technical Service Project of Eighth Geological Brigade of Hebei Bureau of Geology and Mineral Resources Exploration (KJ2022-021).

Data Availability Statement: No new data were created or analyzed in this study. Data sharing is not applicable to this article.

Conflicts of Interest: The authors declare no conflict of interest.

References

1. Hadamard, J. *Lectures on Cauchy Problems in Linear Partial Differential Equations*; Yale University Press: New Haven, CT, USA, 1923.
2. Dippon, J.; Gwinner, J.; Khan, A.A.; Sama, M. A new regularized stochastic approximation framework for stochastic inverse problems. *Nonlinear Anal. Real World Appl.* **2023**, *73*, 103869. [CrossRef]
3. Dambrine, M.; Khan, A.A.; Sama, M. A stochastic regularized second-order iterative scheme for optimal control and inverse problems in stochastic partial differential equations. *Philos. Trans. R. Soc. A* **2022**, *380*, 20210352. [CrossRef] [PubMed]
4. Georgiev, S.; Vulkov, L. Parameters identification and numerical simulation for a fractional model of honeybee population dynamics. *Fractal Fract.* **2023**, *7*, 311. [CrossRef]
5. Georgiev, S.G.; Vulkov, L.G. Coefficient identification in a SIS fractional-order modelling of economic losses in the propagation of COVID-19. *J. Comput. Sci.* **2023**, *69*, 102007. [CrossRef] [PubMed]
6. Shivanian, E.; Jafarabadi, A. The numerical solution for the time-fractional inverse problem of diffusion equation. *Eng. Anal. Bound. Elem.* **2018**, *91*, 50–59. [CrossRef]
7. Abdelwahed, M.; BenSaleh, M.; Chorfi, N.; Hassine, M. An inverse problem study related to a fractional diffusion equation. *J. Math. Anal. Appl.* **2022**, *512*, 126145. [CrossRef]

8. Zhang, Z.Y.; Zhang, H.; Liu, Y.; Li, J.Y.; Liu, C.B. Generalized conditional symmetry enhanced physics-informed neural network and application to the forward and inverse problems of nonlinear diffusion equations. *Chaos Soliton. Fract.* **2023**, *168*, 113169. [CrossRef]
9. Shivanian, E.; Jafarabadi, A. The spectral meshless radial point interpolation method for solving an inverse source problem of the time-fractional diffusion equation. *Appl. Numer. Math.* **2018**, *129*, 1–25. [CrossRef]
10. BenSalah, M. Topological sensitivity analysis method in identifying of point sources via time-fractional diffusion equation. *Acta Appl. Math.* **2022**, *181*, 4. [CrossRef]
11. Seblani, Y.E.; Shivanian, E. New insight into meshless radial point Hermite interpolation through direct and inverse 2-D reaction-diffusion equation. *Eng. Comput.* **2021**, *37*, 3605–3613. [CrossRef]
12. BenSalah, M.; Hassine, M. Inverse source problem for a diffusion equation involving the fractional spectral Laplacian. *Math. Methods Appl. Sci.* **2021**, *44*, 917–936. [CrossRef]
13. Rodrigues, F.A.; Orlande, H.R.; Dulikravich, G.S. Simultaneous estimation of spatially dependent diffusion coefficient and source term in a nonlinear 1D diffusion problem. *Math. Comput. Simul.* **2004**, *66*, 409–424. [CrossRef]
14. Rashedi, K. A numerical solution of an inverse diffusion problem based on operational matrices of orthonormal polynomials. *Math. Methods Appl. Sci.* **2021**, *44*, 12980–12997. [CrossRef]
15. Lukyanenko, D.V.; Grigorev, V.B.; Volkov, V.T.; Shishlenin, M.A. Solving of the coefficient inverse problem for a nonlinear singularly perturbed two-dimensional reaction-diffusion equation with the location of moving front data. *Comput. Math. Appl.* **2019**, *77*, 1245–1254. [CrossRef]
16. Garmatter, D.; Haasdonk, B.; Harrach, B. A reduced basis Landweber method for nonlinear inverse problems. *Inverse Probl.* **2016**, *32*, 035001. [CrossRef]
17. Al-Mahdawi, H.K.I.; Alkattan, H.; Abotaleb, M.; Kadi, A.; El-kenawy, E.S.M. Updating the landweber iteration method for solving inverse problems. *Mathematics* **2022**, *10*, 2798. [CrossRef]
18. Bergou, E.H.; Diouane, Y.; Kungurtsev, V. Convergence and complexity analysis of a Levenberg–Marquardt algorithm for inverse problems. *J. Optim. Theory Appl.* **2020**, *185*, 927–944. [CrossRef]
19. Jiang, Y.; Nakamura, G. Convergence of Levenberg-Marquardt method for the inverse problem with an interior measurement. *J. Inverse Ill-Posed Probl.* **2019**, *27*, 195–215. [CrossRef]
20. Karabanova, O.V.; Kokurin, M.Y.; Kozlov, A.I. Finite dimensional iteratively regularized Gauss–Newton type methods and application to an inverse problem of the wave tomography with incomplete data range. *Inverse Probl. Sci. Eng.* **2020**, *28*, 637–661. [CrossRef]
21. Bakushinsky, A.; Smirnova, A. A study of frozen iteratively regularized Gauss–Newton algorithm for nonlinear ill-posed problems under generalized normal solvability condition. *J. Inverse Ill-Posed Probl.* **2020**, *28*, 275–286. [CrossRef]
22. Margenberg, N.; Hartmann, D.; Lessig, C.; Richter, T. A neural network multigrid solver for the Navier-Stokes equations. *J. Comput. Phys.* **2022**, *460*, 110983. [CrossRef]
23. Antonietti, P.F.; Sarti, M.; Verani, M. Multigrid algorithms for hp-discontinuous Galerkin discretizations of elliptic problems. *SIAM J. Numer. Anal.* **2015**, *53*, 598–618. [CrossRef]
24. Medina, A.C.; Schmid, R. Solution of high order compact discretized 3D elliptic partial differential equations by an accelerated multigrid method. *J. Comput. Appl. Math.* **2019**, *350*, 343–352. [CrossRef]
25. Muratova, G.; Martynova, T.; Andreeva, E.; Bavin, V.; Wang, Z.Q. Numerical solution of the Navier-Stokes equations using multigrid methods with HSS-based and STS-based smoothers. *Symmetry* **2020**, *12*, 233. [CrossRef]
26. Al-Mahdawi, H.K.I.; Abotaleb, M.; Alkattan, H.; Tareq, A.M.Z.; Badr, A.; Kadi, A. Multigrid method for solving inverse problems for heat equation. *Mathematics* **2022**, *10*, 2802. [CrossRef]
27. Al-Mahdawi, H.K.; Sidikova, A.I.; Alkattan, H.; Abotaleb, M.; Kadi, A.; El-Kenawy, E.S.M. Parallel multigrid method for solving inverse problems. *MethodsX* **2022**, *9*, 101887. [CrossRef]
28. Ye, J.C.; Bouman, C.A.; Webb, K.J.; Millane, R.P. Nonlinear multigrid algorithms for Bayesian optical diffusion tomography. *IEEE Trans. Image Process.* **2001**, *10*, 909–922.
29. Oh, S.; Milstein, A.B.; Bouman, C.A.; Webb, K.J. A general framework for nonlinear multigrid inversion. *IEEE Trans. Image Process.* **2004**, *14*, 125–140.
30. Li, S.; Montcel, B.; Yuan, Z.; Liu, W.; Vray, D. Multigrid-based reconstruction algorithm for quantitative photoacoustic tomography. *Biomed. Opt. Express* **2015**, *6*, 2424–2434. [CrossRef]
31. Javaherian, A.; Holman, S. A multi-grid iterative method for photoacoustic tomography. *IEEE Trans. Med. Imaging* **2016**, *36*, 696–706. [CrossRef]
32. Braun, E.C.; Bretti, G.; Natalini, R. Parameter estimation techniques for a chemotaxis model inspired by Cancer-on-Chip (COC) experiments. *Int. J. Non-Linear Mech.* **2022**, *140*, 103895. [CrossRef]
33. Bretti, G.; De Ninno, A.; Natalini, R.; Peri, D.; Roselli, N. Estimation algorithm for a hybrid PDEODE model inspired by immunocompetent Cancer-on-Chip experiment. *Axioms* **2021**, *10*, 243. [CrossRef]
34. Edjlali, E.; Bérubé-Lauzière, Y. Lq-Lp optimization for multigrid fluorescence tomography of small animals using simplified spherical harmonics. *J. Quant. Spectrosc. Radiat. Transf.* **2018**, *205*, 163–173. [CrossRef]
35. Liu, T. A nonlinear multigrid method for inverse problem in the multiphase porous media flow. *Appl. Math. Comput.* **2018**, *320*, 271–281. [CrossRef]

36. Jeong, D.; Li, Y.; Choi, Y.; Moon, K.S.; Kim, J. An adaptive multigrid technique for option pricing under the Black-Scholes model. *J. Korean Soc. Ind. Appl. Math.* **2013**, *17*, 295–306. [CrossRef]
37. Clarke, N.; Parrott, K. Multigrid for American option pricing with stochastic volatility. *Appl. Math. Financ.* **1999**, *6*, 177–195. [CrossRef]
38. Vignoli, G.; Fiandaca, G.; Christiansen, A.V.; Kirkegaard, C.; Auken, E. Sharp spatially constrained inversion with applications to transient electromagnetic data. *Geophys. Prospect.* **2015**, *63*, 243–255. [CrossRef]
39. Babadagli, T.; Al-Salmi, S.J.S.R.E. A review of permeability-prediction methods for carbonate reservoirs using well-log data. *SPE Reserv. Eval. Eng.* **2004**, *7*, 75–88. [CrossRef]
40. Lin, T.T.; Lin, X.X.; Yang, Z.J.; Wan, L.; Zhao, J.; Zhang, X.F.; Hao, W.J.; Zhang, Q. Joint and laterally constrained inversion of surface MRS and TEM data. *Chin. J. Geophys.* **2017**, *60*, 833–842.
41. Fournier, A.; Clerget, C.H.; Bharadwaj, P.; Merciu, A.; Skar, G. A seismoelectric inverse problem with well-log data and borehole-confined acquisition. In Proceedings of the SEG International Exposition and Annual Meeting, San Antonio, TX, USA, 15–20 September 2019; p. SEG-2019-3216905.
42. Behroozmand, A.A.; Auken, E.; Fiandaca, G.; Christiansen, A.V. Improvement in MRS parameter estimation by joint and laterally constrained inversion of MRS and TEM data. *Geophysics* **2012**, *77*, WB191–WB200. [CrossRef]
43. Dall'Aglio, A.; Orsina, L. Existence results for some nonlinear parabolic equations with nonregular data. *Differ. Integral Equ.* **1992**, *5*, 1335–1354. [CrossRef]
44. Prignet, A. Existence and uniqueness of "entropy" solutions of parabolic problems with L^1 data. *Nonlinear Anal. TMA* **1997**, *28*, 1943–1954. [CrossRef]
45. Boccardo, L.; Porzio, M.M.; Primo, A. Summability and existence results for nonlinear parabolic equations. *Nonlinear Anal. TMA* **2009**, *71*, 978–990. [CrossRef]
46. Abdellaoui, M.; Azroul, E.; Redwane, H. Existence results for a class of nonlinear parabolic equations of generalized porous medium type with measure data. *Ric. Mat.* **2023**, *72*, 453–490. [CrossRef]
47. Tatar, S.; Ulusoy, S. An inverse problem for a nonlinear diffusion equation with time-fractional derivative. *J. Inverse Ill-Posed Probl.* **2017**, *25*, 185–193. [CrossRef]
48. Egger, H.; Pietschmann, J.F.; Schlottbom, M. On the uniqueness of nonlinear diffusion coefficients in the presence of lower order terms. *Inverse Probl.* **2017**, *33*, 115005. [CrossRef]
49. Abtahi, M.; Pourgholi, R.; Shidfar, A. Existence and uniqueness of a solution for a two dimensional nonlinear inverse diffusion problem. *Nonlinear Anal. TMA* **2011**, *74*, 2462–2467. [CrossRef]
50. Zhao, J.; Liu, T.; Liu, S. Identification of space-dependent permeability in nonlinear diffusion equation from interior measurements using wavelet multiscale method. *Inverse Probl. Sci. Eng.* **2014**, *22*, 507–529. [CrossRef]